Bioresource Technology 315 (2020) 123797

Contents lists available at ScienceDirect

Bioresource Technology

journal homepage: www.elsevier.com/locate/biortech

# A highly efficient strategy for enhancing the adsorptive and magnetic capabilities of biochar using Fenton oxidation

Shuang Xu[a], Jihui Li[a,b,c,*], Zhibing Yin[a], Sen Liu[a], Siyao Bian[a], Yucang Zhang[a]

[a] Key Laboratory of Ministry of Education for Advanced Materials in Tropical Island Resources, School of Chemical Engineering and Technology, Hainan University, Haikou 570228, PR China
[b] School of Science, Hainan University, Haikou 570228, PR China
[c] Hainan Provincial Key Lab of Fine Chem, School of Chemical Engineering and Technology, Hainan University, Haikou 7570228, PR China

## GRAPHICAL ABSTRACT

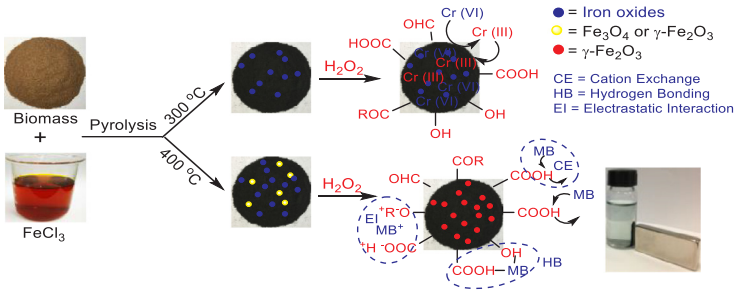


## ARTICLE INFO

*Keywords:*
Biochar
Fenton oxidation
Adsorptive and magnetic capabilities
Methylene blue
Chromium

## ABSTRACT

Fenton modification, involving iron-promoted pyrolysis followed by $H_2O_2$ oxidation, was first employed to improve the adsorptive and magnetic capabilities of biochar. Modified biochars were prepared from rubber tree bark and coconut shell through iron-promoted pyrolysis and subsequent $H_2O_2$ oxidation, and their adsorption behaviors toward Cr (VI) and MB were evaluated in aqueous solution. The modified biochars pyrolyzed at 300 and 400 °C displayed much higher adsorption capabilities than corresponding pristine biochars for Cr (VI) and MB, respectively, ascribing to introduction of COOH, C═O and C–O groups by Fenton oxidation. More importantly, saturation magnetization could be enhanced by transforming nonmagnetic iron oxides into γ-$Fe_2O_3$ through $H_2O_2$ oxidation. The removal of Cr (VI) and MB could be primarily contributed to the adsorption of biochar matrix by reduction/hydrogen bonding/cation exchange/electrostatic interaction and hydrogen bonding/cation exchange/electrostatic interaction, respectively. This would provide a novel and efficient strategy for making highly adsorptive magnetic biochar.

## 1. Introduction

Magnetic modification is an attractive strategy for overcoming the difficulty in solid–liquid separation of biochar, provides great advantages for water treatment using biochar (Wang et al., 2019; Yi et al., 2020). Mostly, it is realized by introducing magnetic medium through either pyrolysis (Han et al., 2016; Trakal et al., 2016) or post-coating (Mohan et al., 2014a; Wang et al., 2017) using low-cost and less toxic iron salts as precursor. One common method is zero-valent iron (nZVI) doped modification, in which ZVI is generated on biochar matrix

* Corresponding author at: Key Laboratory of Ministry of Education for Advanced Materials in Tropical Island Resources, School of Chemical Engineering and Technology, Hainan University, Haikou 570228, PR China.
*E-mail address:* lijihui@hainanu.edu.cn (J. Li).

https://doi.org/10.1016/j.biortech.2020.123797
Received 17 May 2020; Received in revised form 1 July 2020; Accepted 4 July 2020
Available online 09 July 2020
0960-8524/ 

through reduction of iron species by $NaBH_4$ (Wang et al., 2017; Yang et al., 2018). The modification can lead to the increase of adsorption capability due to the complementation of ZVI and biochar matrix (Devi & Saroha, 2014). Comparing to ZVI doped modification, magnetic iron oxide-doped modification should be more attractive for practical application as producing oxidatively stable $Fe_3O_4$- and/or γ-$Fe_2O_3$-doped biochar (Mohan et al., 2014b; Zhang et al., 2013). Great advance has been made in this magnetic modification in the past decade, but some defects such as generation of nonmagnetic iron species (Reguyal et al., 2017) and loss of active adsorption sites (Karunanayake et al., 2018; Reguyal et al., 2017) still remain to be resolved.

As generating oxygen-containing groups which have good affinity to heavy metals and organic molecules (Huff & Lee, 2016; Mandal et al., 2017), oxidation is considered to be a promising technology for enhancing the adsorption capability of biochar. Especially, $H_2O_2$ oxidation, which can tune the physiochemical properties of biochar by introducing oxygen containing groups (Huff & Lee, 2016) as well as modulating morphology and pore structure (Tan et al., 2011), is attractive for environment remediation as producing less harmful residues. In last decades, many $H_2O_2$ modifications were developed to engineer different nonmagnetic biochars for removal of heavy metals such as $Cu^{2+}$, $Pd^{2+}$, $Cd^{2+}$ and Ni in aqueous solution (Wang et al., 2018; Xue et al., 2012; Zuo et al., 2016). In addition, $H_2O_2$-pretreatment and microwave activation were combined to enhance the adsorption capability of Prosopis juliflora biochar for remazol brilliant blue and methylene blue (Nair & Vinu, 2016). However, high concentration of $H_2O_2$ was usually required for these modifications and low efficiency was obtained for improving adsorption capability of biochar due to the weak oxidizing ability of $H_2O_2$, seriously restricting wide application of $H_2O_2$ modification.

Fenton oxidation, an iron-catalyzed advanced oxidation, can rapidly generate highly active HO· radical to oxidize different functional groups into diversified oxygen-containing groups (Zhu et al., 2019). The combination of iron modification and $H_2O_2$ modification (Fenton modification) should complement each other for regulating the physiochemical properties of biochar. $H_2O_2$ oxidation of biochar matrix can be promoted by iron significantly, generating a large number of oxygen-containing groups including OH, COOH and C═O on biochar (eqs (1), (2)). Meanwhile, $H_2O_2$ decomposition (eq (3)) can also be accelerated to massively produce $O_2$ for modulating the morphology of biochar. On the other hand, nonmagnetic iron species such as ferrous oxides and ferric hydroxides should be transformed into γ-$Fe_2O_3$ with oxidization and dehydration of $H_2O_2$ (eq (4)), benefiting to enhancing saturation magnetization as well as increasing active adsorption sites (Zhang et al., 2020). Hence, Fenton modification can multi-directionally regulate the physiochemical properties of biochar, providing a promising strategy for addressing the drawbacks in both magnetic iron oxide-doped modification and $H_2O_2$ modification simultaneously. Nevertheless, Fenton oxidation has been less explored for precisely engineering biochar for efficient removal of pollutants by now.

$$Fe^{2+} + H_2O_2 \rightarrow Fe^{3+} + HO^- + HO\cdot \quad (1)$$

$$HO\cdot + BC \rightarrow OBC \quad (2)$$

$$Fe^{3+} + H_2O_2 \rightarrow Fe^{2+} + O_2 + H^+ \quad (3)$$

$$Fe_xO_y \ or \ Fe(OH)_z + H_2O_2 \rightarrow \gamma - Fe_2O_3 \quad (4)$$

Dye and heavy metal pollution has posed a serious threat to human and ecological environment. Hexavalent chromium (Cr (VI)) and methylene blue (MB) are common contaminants in aquatic environments by industrialization such as mining, electroplating, textile and dyeing (Qada et al., 2006; Pradhan et al., 2017). As a low-cost and renewable adsorbent, biochar has been widely applied to remove Cr (VI) (Chen et al., 2015; Nasuha & Hameed, 2011; Zhao et al., 2018) and MB (Daneshvar et al., 2017; Zhang & Gao, 2013) from aqueous solution in the past decade. Importantly, considerable progress has already been made in preparation of magnetic biochar for treating Cr (VI)-contaminated water due to the advantage of easy separation. For example, ZVI/biochar composites were prepared for adsorbing Cr (VI) with relatively low adsorption capabilities (Zhou et al., 2014), where the biochars mainly acted as supporter and electron-transfer medium. Multi-step synthesized $Fe_3O_4$- and ϒ-$Fe_2O_3$-doped magnetic biochars were demonstrated to exhibit moderate and high adsorption capabilities toward Cr (VI) (Han et al., 2016; Shi et al., 2018), respectively. Recently, surface functionalization was developed for enhancing the adsorption capabilities of $Fe_3O_4$/biochar and ϒ-$Fe_2O_3$/biochar composites (Mian et al., 2018; Yin et al., 2020), confirming biochar matrix could contribute greatly to the adsorption capability of magnetic biochar. By contrast, despite ZVI- and iron oxide-doped magnetic biochars were also made for adsorbing MB, inferior adsorption capabilities were obtained (Mubarak et al., 2015; Nasuha & Hameed, 2011).

Herein, Fenton oxidation was employed to engineer two biochars made from bio-wastes rubber tree bark and coconut shell for removing Cr (VI) and MB in aqueous solution. For comparison, the corresponding $H_2O_2$– and $FeCl_3$-modified biochars were also prepared and their adsorption capabilities were estimated. The objectives of this study were to: 1) establish a general method for improving the adsorption capability of biochar toward Cr (VI) and MB using Fenton oxidation; 2) evaluate Fenton oxidation for enhancing saturation magnetization of magnetic biochar; 3) illuminate the adsorption mechanism of the modified biochars toward Cr (VI) and MB.

## 2. Materials and methods

### 2.1. Materials

The rubber tree bark and coconut shell were collected from a farm around Danzhou city in Hainan province of China. The chemicals including HCl, KOH, $H_2SO_4$, $FeCl_3$, $H_2O_2$, MB and $K_2Cr_2O_7$ were analytical reagent grade and purchased from Aladdin and Macklin. Different concentrations of Cr (VI) and MB solutions were prepared by dissolving $K_2Cr_2O_7$ and MB in deionized water (water treatment system, LD-UPW-20, Leading, Shanghai, China), respectively.

### 2.2. Preparation of biochars

The rubber tree bark was crushed into powder (60 mesh). The powder (10 g) and 2 mol/L $FeCl_3$ solution (80 mL) were mixed and magnetically stirred at room temperature for 2 h, then aged at 70 °C for 30 min. The mixture was filtered to get iron-loaded biomass, and dried at 60 °C for 48 h. The dried sample was ground and pyrolyzed at the target temperature (200 °C, 300 °C, 400 °C, 500 °C, 600 °C) for 1 h with 5 °C/min heating rate under nitrogen. After cooling to room temperature, the sample was washed and dried at 60 °C to get Fe-modified biochar. The biochars were named as Fe200, Fe300, Fe400, Fe500 and Fe600 based on pyrolysis temperature, respectively. The Fe-modified biochar (3 g) was treated with $H_2O_2$ solution (60 mL) for 2 h, washed and dried at 60 °C to obtain Fenton-modified biochar. The Fenton-modified biochars were named as Fe-$H_2O_2$200, Fe-$H_2O_2$300, Fe-$H_2O_2$400, Fe-$H_2O_2$500 and Fe-$H_2O_2$600 according to pyrolysis temperature, respectively. The pristine biochar was prepared through pyrolysis of rubber tree bark powder directly at different temperatures (200 °C, 300 °C, 400 °C, 500 °C, 600 °C) and called P200, P300, P400, P500 and P600, respectively. The P300 and P400 were oxidized with $H_2O_2$ to mkae $H_2O_2$-modified biochars ($H_2O_2$300 and $H_2O_2$400). They were also modified by reacting with $FeCl_3$ (2 M) and $H_2O_2$ in 3/7/60 (g/mL/mL) ratio to make direct Fenton oxidative biochars (Marked as P300-DF and P400-DF). Besides, pristine coconut shell biochars were prepared at 300 and 400 °C (called CP300 and CP400). The corresponding $FeCl_3$- and Fenton-modified biochars were also made using the above modification procedures (labeled as CFe300, CFe400, CFe-$H_2O_2$300 and CFe-$H_2O_2$400).

### 2.3. Characterization of rubber tree bark biochar

The textural property was analyzed using $N_2$ sorption/desorption isotherms at 77 K on a surface area and porosity analyzer (Micromeritics ASAP 2460, USA). The surface area was calculated by the Brunauere Emmentte Teller (BET) method, and both pore volume and average pore size were calculated by Barret-Joyner-Halenda (BJH) method. The element content was analyzed with organic element analyzer (Thermo Scientific Flash 2000 CHNS/O, America) and inductive couple plasma (ICP) elemental analyzer (Agilent ICPOES 730, America). The morphology was observed through scanning electron microscope (SEM, Phenom Prox, Holland) with energy-dispersive X-ray spectroscopy (EDS). The functional groups were characterized by Fourier transform and infrared (FTIR) spectrum (Bruker Tensor 27, Germany) using 2 mg biochar and 1000 mg KBr. The surface composition was characterized using X-ray photoelectron spectrum (XPS) (Thermo Scientific Escalab 250Xi, America). The crystallinity was determined on an X-ray diffractometer (Brucker D8 Adavance, Germany) with Cu $K_\alpha$ radiation over a $2\theta$ collection range of 10–90 °.

### 2.4. Adsorption experiments

Briefly, biochar and adsorbate solution were added in conical flask and shaken at 180 rpm for desired time, then the mixture was filtered through a membrane filter for analyzing adsorbate concentration. For the kinetic experiments, the adsorption was carried out using the time intervals (0.5, 1, 2, 4, 8, 12, 16, 24, 32, 40 and 48 h). The adsorption isotherm experiments were performed using a series of initial concentrations (Cr: 100, 150, 200, 250, 300, 350, 400, 450, 500 mg/L; MB: 2.5, 5, 10, 15, 25, 50, 75 and 100 mg/L were applied for P400; 25, 50, 75, 100, 150, 200, 250, 300 and 350 mg/L were employed for Fe-$H_2O_2$400).

The MB and Cr (VI) concentrations were measured by UV–vis spectrophotometer (MAPADA UV-3300PC, Shanghai) at 665 nm and 540 nm [1.5-diphenylcarbazide was used as indicator for Cr (VI)], respectively. The adsorption capability of biochar was determined by the difference of concentrations before and after adsorption.

### 2.5. Regeneration of biochar

The regeneration of P300 and Fe-$H_2O_2$300 was performed in a pH13 NaOH solution (1/1 mg/mL ratio) for 16 h at 25 °C. The regeneration of PBC400 and FOBC400 was carried out in common solvents including $CH_3CN$, HCl solution and EtOH/acetic acid (9/1 vol ratio) using 1/2 (mg/mL) ratio for 24 h at 25 °C.

## 3. Results and discussion

### 3.1. Characterization

As shown in Table 1, both pristine and Fenton-modified biochars prepared at 300 and 400 °C possessed mesopore structure with inferior specific surface area (SSA). The Fenton-modified biochar had higher SSA and pore volume (PV) than the prisinte biochar pyrolyzed at the same temperature.

The element analysis showed that Fenton-modified biochar contained more Fe and O than corresponding pristine biochar (Table 2). Comparing to Fe-modified biochar, Fenton-modified biochar had much less Fe, implying $H_2O_2$ oxidation caused Fe release from biochar. It was noted that the O/C ratio of Fe-$H_2O_2$400 was much higher than that of P400 and Fe400, demonstrating organic oxygen containing groups could be generated on biochar matrix by Fenton oxidation.

**Table 1**
Physical properties of biocahr.

| Biochar[a] | SSA ($m^2$/g) | PV ($cm^3$/g) | PD (nm) |
|---|---|---|---|
| P300 | 1.11 | 0.00212 | 6.83 |
| Fe-$H_2O_2$300 | 2.63 | 0.01218 | 18.46 |
| P400 | 2.11 | 0.00558 | 12.24 |
| Fe-$H_2O_2$400 | 3.47 | 0.00859 | 12.42 |

The common functional groups including –OH (3448 $cm^{-1}$, streching vibration), aliphatic C–H (2925 $cm^{-1}$, streching vibration), C=O/aromatic C=C (1624 $cm^{-1}$, streching vibrations), C=C (1435 $cm^{-1}$, streching vibration), COOH (1383 $cm^{-1}$ bending vibiration) (Song et al., 2014), aliphatic C–O (1058 $cm^{-1}$, streching vibration) were observed on the pristine biochars prepared at 300 and 400 °C (E-supplementary data for this work can be found in e-version of this paper online). (Özçimen & Ersoy-Meriçboyu, 2010) Calcium oxalate (1317 and 781 $cm^{-1}$), (Tan et al., 2003) which might be derived from calcium salts on banana pseudostem, was also found on them. In comparison, the $H_2O_2$-modified biochars had weaker C–O streching vibration peaks due to $H_2O_2$ oxidation. Obviously, the characteristic peaks of calcium oxalate were hardly observed on Fe-modified biochars, indicating the formation of calcium oxalate was completely inhibited during $FeCl_3$-promoted pyrolysis. Fe400 showed much stronger aromatic C–H bending peak (874 $cm^{-1}$) than P400, as aromatic structure was formed through dehydration of $FeCl_3$ at high temperature. As expected, new COOH (1710 or 1707 $cm^{-1}$, streching vibriation) and C-O (1058 or 1246 $cm^{-1}$, streching vibriation) groups were produced with Fenton modification. The C-O peak of Fenton-modified biochar shifted to higher wavenumber as pyrolyzed at relatively high temperature (400 °C) attributing to formation of aromatic structure. These suggested that Fenton oxidation surpassed single iron-promoted pyrolysis and $H_2O_2$ oxidation for generating oxygen containing groups on biochar.

The XPS analysis results were listed in Table 3. The Fenton-modified biochar had higher surface O content than corresponding prisinte biochar. Iron was hardly detected on the surfaces of Fenton-modified biochar. Furthermore, the deconvolution of C 1 s peak showed that oxygen-containing groups including C-O (286.2 ev), C=O (287.2ev) and COO (288.8 ev) (Yao et al., 2010) of Fenton-modified biochar were all more than that of corresponding pristine biochar. Therefore, various oxygen containing groups could be successfully introduced on the surface of biochar through Fenton oxidation.

SEM images demonstrated that pristine biochars were composed of irregular microparticles with rough surface (E-supplementary data for this work can be found in e-version of this paper online). Relatively smooth surfaces were obtained for Fenton-modified biochars comparing to pristine and Fe-modified biochars, indicating rough surface was damaged by Fenton oxidation. Obviously, a considerable amount of mesopores were generated on the microparticles of Fenton-modified biochars, thereby higher SSA and PV were obtained (Table 1). On the contrast, direct Fenton oxidation, where prstine biochar reacted with $FeCl_3$ and $H_2O_2$, rarely produced new mesopores even though $H_2O_2$ decomposition intensively occurred. Similarly, iron-promoted pyrolysis also hardly produced mesopores (E-supplementary data for this work can be found in e-version of this paper online). This indicated that the formation of porous structure mainly resulted from iron-promoted $H_2O_2$ decomposition taking place inside biochar matrix. In accordance with element analysis, EDS spectra also proved that the iron oxides and oxygen containing groups were incorporated onto pristine biochar with Fenton modification.

Pristine, Fe-modified and Fenton-modified biochars prepared at 300 and 400 °C were characterized by XRD spectra (E-supplementary data for this work can be found in e-version of this paper online). The multiple diffraction peaks at $2\theta$ = 14.93, 24.39, 30.11, 38.18° were obtained for pristine biochars. These peaks were attributed to calcium oxalate hydrates (Kırboğa & Öner, 2009; Ouyang et al., 2004). Broad peaks around $2\theta$ = 20.0° were also observed on them, indicating the presence of amorphous carbon (Xiong et al., 2018). Calcium oxalate

**Table 2**
Element analysis of biochar.

| Sample | C (wt%) | H (wt%) | O (wt%) | N (wt%) | Fe (wt%) | O/C[a] | Fe/C[a] |
|---|---|---|---|---|---|---|---|
| P300 | 57.25 | 4.82 | 18.38 | 1.10 | 0.02 | 0.21 | 0.000 |
| Fe300 | 52.63 | 4.64 | 31.57 | 1.08 | 5.21 | 0.40 | 0.021 |
| Fe-$H_2O_2$300 | 58.45 | 5.19 | 20.70 | 0.69 | 1.00 | 0.24 | 0.004 |
| P400 | 62.09 | 3.78 | 20.85 | 0.86 | 0.07 | 0.22 | 0.000 |
| Fe400 | 67.83 | 3.68 | 17.64 | 1.21 | 3.92 | 0.17 | 0.012 |
| Fe-$H_2O_2$400 | 57.45 | 3.48 | 30.93 | 0.62 | 1.68 | 0.36 | 0.006 |

[a] *mol ratio.*

**Table 3**
Surface element and functional group composition.

| Biochar | Element ratio | | | | Functional group (binding energy, eV) | | | |
|---|---|---|---|---|---|---|---|---|
| | O/C | N/C | Ca/C | Si/C | C–C/C=C (284.8) | C–O (286.2) | C=O (287.2) | O–C=O (288.8) |
| P300 | 29.84 | 0.00 | 0.12 | 3.44 | 1.00 | 0.20 | 0.03 | 0.12 |
| Fe-$H_2O_2$300 | 31.23 | 1.19 | 0.00 | 2.46 | 1.00 | 0.24 | 0.09 | 0.15 |
| P400 | 24.09 | 1.26 | 1.99 | 0.00 | 1.00 | 0.18 | 0.03 | 0.09 |
| Fe-$H_2O_2$400 | 31.83 | 1.30 | 0.00 | 0.00 | 1.00 | 0.34 | 0.04 | 0.16 |

hydrates weren't produced with Fe-promoted pyrolysis as their feature diffraction peaks were hardly detected on the Fe-modified biochars, which was in consistence with FTIR analysis. Comparing to Fe300, additional diffraction peaks at $2\theta$ = 30.0°, 35.3°, 43.0°, 56.8° and 62.4°, which could be assigned to $Fe_3O_4$ (Duan et al., 2017) or γ-$Fe_2O_3$ (Zhang et al., 2013), were observed on Fe400. This indicated that the formation of magnetic iron oxide required high pyrolysis temperature (Han et al., 2016). Interestingly, subsequent Fenton oxidation generated crystalline graphene structure as a sharp peak of graphitic carbon at $2\theta$ = 26.60° (JCPDS75-1621) (Lai et al., 2018; Zhi et al., 2014) was detected on Fenton-modified biochars. Moreover, it produced new magnetic iron oxide on Fe-$H_2O_2$400 as stronger diffraction peaks of $Fe_3O_4$ or γ-$Fe_2O_3$ were detected. Whereas, the magnetic iron oxides were scarcely generated on Fe-$H_2O_2$300. This suggested that the preformed magnetic iron oxide on biochar might act as an inducer for producing new one. More importantly, the saturation magnetization of Fe-$H_2O_2$400 was enhanced from 0.219 to 1.076 emu/g (Fig. 3c) with Fenton oxidation even though iron reduced (Table 2). It could be concluded that the magnetic iron of Fe-$H_2O_2$400 should be γ-$Fe_2O_3$ rather than $Fe_3O_4$ as low valence iron oxides including $Fe_3O_4$ could be oxidized into γ-$Fe_2O_3$ by $H_2O_2$. In a word, Fenton oxidation could be a promising method for improving the magnetic capability of magnetic biochar by converting nonmagnetic iron species into magnetic γ-$Fe_2O_3$.

### 3.2. Adsorption of Cr (VI) and MB

#### 3.2.1. Effect of preparation parameters on adsorption capability

As shown in Fig. 1a, the optimal pyrolysis temperature was 300 °C for adsorption of Cr (VI) as Fe-$H_2O_2$300 displayed much higher adsorption capability than other pristine and Fenton-modified biochars. Different $H_2O_2$ concentrations (5, 10, 20 wt%) were found to be effective for improving the adsorption capability of Cr (VI) and 10 wt% $H_2O_2$ gave highest adsorption capability (Fig. 1b). For adsorption of MB, the optimized pyrolysis temperature and $H_2O_2$ concentration were 400 °C and 20 wt% $H_2O_2$, respectively (Fig. 1c-d). It was noted that the Fe-$H_2O_2$400 exhibited 9.8 times higher adsorption capability than P400. Thereby, Fenton modification is highly efficient for improving the adsorption capabilities for both Cr (VI) and MB. By contrast, iron-promoted pyrolysis only leaded to sharp decrease in adsorption of Cr (VI) and MB even incorporating iron oxides (Zhang et al., 2020). $H_2O_2$ post-oxidation caused significant diminishment and slight increase in adsorption of Cr (VI) and MB, respectively. This demonstrated that Fenton modification outperformed single iron-modification and $H_2O_2$-modification. Besides, post-Fenton oxidation without iron-promoted pyrolysis failed to upgrade the adsorption capabilities of P300 and P400, thereby incorporation of Fe into biochar matrix through pyrolysis was of great importance for enhancing the adsorption capability of biochar. In the following experiments, the pristine and Fenton-modified biochars prepared at 300 and 400 °C were selected to study the adsorption behaviors of MB and Cr (VI), respectively.

#### 3.2.2. The effect of initial pH on adsorption capability

The adsorption capabilities of P300 and Fe-$H_2O_2$300 toward Cr (VI) sharply decreased as increasing pH from 2 to 5 (Fig. 2a). This might be attributed to: 1) formation of $HCrO_4^-$ and electropositive biochar surface, 2) increasing oxidizability of Cr (VI) at low pH (Zhou et al., 2016). For adsorption of MB, P400 always displayed inferior adsorption capability without impact of pH, and Fe-$H_2O_2$400 showed slightly increasing adsorption capability with the increase of pH from 3 to 9 (Fig. 2b). Additionally, the pH change of MB solution was recorded after adsorption to understand the adsorption process (Fig. 2c). The pH increased as performing the adsorption of P400 under acidic and nearly neutral conditions. Oppositely, the pH all decreased for Fe-$H_2O_2$400 over a wide pH range from 3 to 9. In particular, the pH sharply decreased to 3.8 while the adsorption was carried out at pH7. This indicated Fe-$H_2O_2$400 displayed strong cation exchange capability for adsorption of MB.

#### 3.2.3. Adsorption kinetics and isotherms

The adsorption kinetics and isotherms of Cr (VI) and MB were depicted in Fig. 3. The adsorption kinetics were better described by pseudo-second order model (PSOM) than pseudo-first order model (PFOM) as PSOM offered good determinant coefficient and slightly higher calculated equilibrium adsorption capability than experimental one (Table 4). The adsorptions were all endothermic processes as the adsorption capabilities of biochars increased with temperature (Fig. 3e-h). The adsorption processes were better stimulated by Langmuir model than Freundich model (Table 4). Fe-$H_2O_2$300 and Fe-$H_2O_2$400 exhibited much higher adsorption capacities than P300 and P400 with 335.57 and 258.14 mg/g maximum adsorption capabilities for Cr (VI) and MB at 45 °C, respectively, surpassed most biochars reported in the literature (Ma et al., 2014; Mian et al., 2018; Shi et al., 2018).

#### 3.2.4. Regeneration of biochar

The regeneration of PBC300 and FOBC300 was performed in aqueous NaOH solution with pH13. Surprisedly, the adsorption capabilities of them increased for first regeneration (Fig. 4a), which could be resulted from the generation of new hydroxyls and carboxyls through hydrolysis of esters (Ding et al., 2016). As recycled for more than one time, both P300 and Fe-$H_2O_2$300 showed decreased adsorption capabilities probably owing to the incomplete desorption of Cr (VI).

The common solvents including $CH_3CN$, HCl solution and EtOH/acetic acid (9/1), which had been demonstrated to be efficient solvents for desorbing MB from carbon materials (Lyu et al., 2020), were used to regenerate P400 and Fe-$H_2O_2$400. However, only a small part of MB

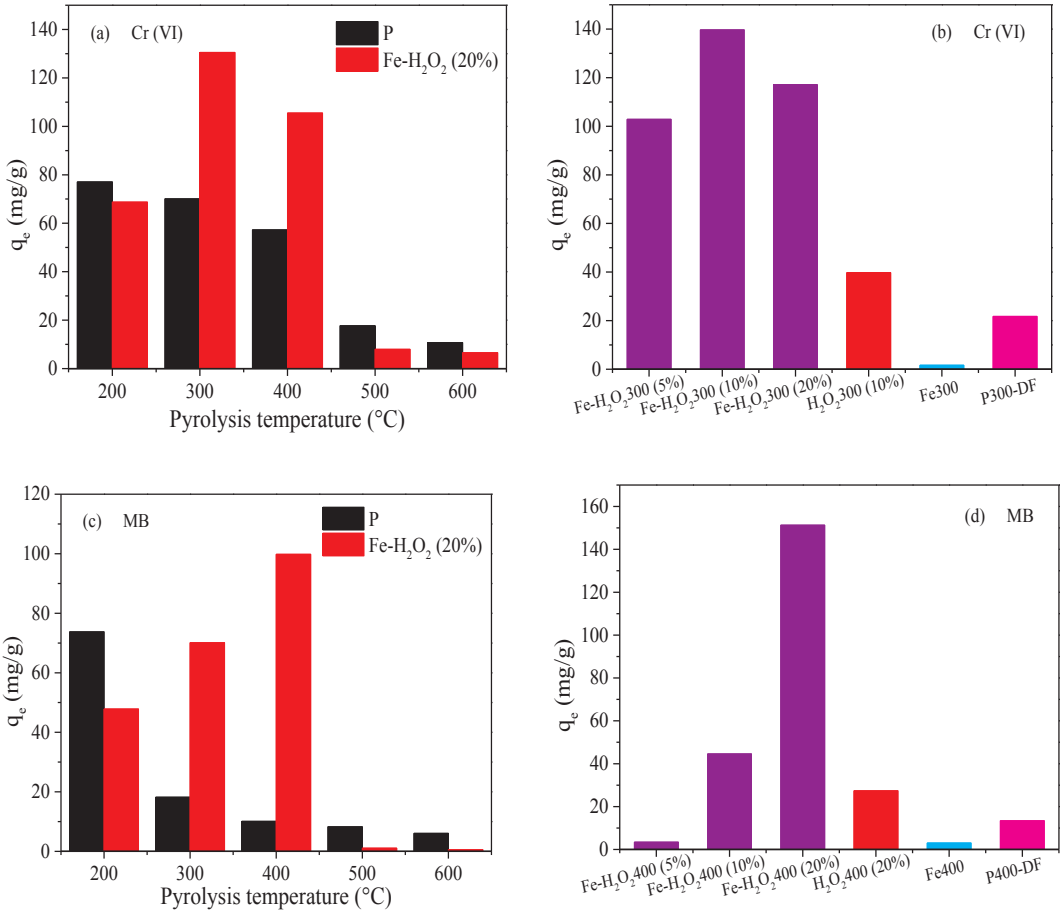


**Fig. 1.** Effect of preparation parameters on adsorption capabilities for Cr (VI) (200 mg/L, 1 g/L, pH2, 24 h (a) or 48 h (b), 25 ℃) and MB (100 mg/L, pH7, 0.5 g/L; 24 h (c) or 48 h (d), 25 ℃).

was desorbed, so the regenerated biochars showed much lower adsorption capabilities (Fig. 4b). This was also demonstrated by the FTIR spectrum of Fe-$H_2O_2$400 after desorption as the feature peaks of MB (1329, 1387 $cm^{-1}$) was still obviously present (E-supplementary data for this work can be found in e-version of this paper online).

### 3.2.5. Adsorption mechanism

The XPS analysis showed that the chromium loaded on P300 was mainly consisted of Cr (III) (Cr $2p_{3/2}$: 577.3 eV, Cr $2p_{1/2}$: 287.0 eV) (Liu et al., 2014; Manning et al., 2007) (E-supplementary data for this work can be found in e-version of this paper online). This indicated the removal of Cr (VI) by P300 was determined by reduction of Cr (VI) to Cr (III). Differently, the chromium fixed on Fe-$H_2O_2$300 was comprised of Cr (III) (Cr $2p_{3/2}$: 577.1 eV, Cr $2p_{1/2}$: 286.7 eV) and Cr (VI) (Cr $2p_{3/2}$: 579.0 eV, Cr $2p_{1/2}$: 288.3 eV) with 67% and 33%, respectively (E-supplementary data for this work can be found in e-version of this paper online). Therefore, the removal of Cr (VI) by Fe-$H_2O_2$300 was attributed to both reduction of Cr (VI) to Cr (III) and sorption of Cr (VI). To gain deep insights into the adsorption mechanism, P300 and Fe-$H_2O_2$300 were examined by FTIR spectra after adsorption. The C-O peaks of the biochars (1100 and 1058 $cm^{-1}$) somewhat decreased (E-supplementary data for this work can be found in e-version of this paper online), suggesting C-O groups could act as reducing sites for removing Cr (VI). The stretching vibration peak of carboxyl (1710 $cm^{-1}$) on

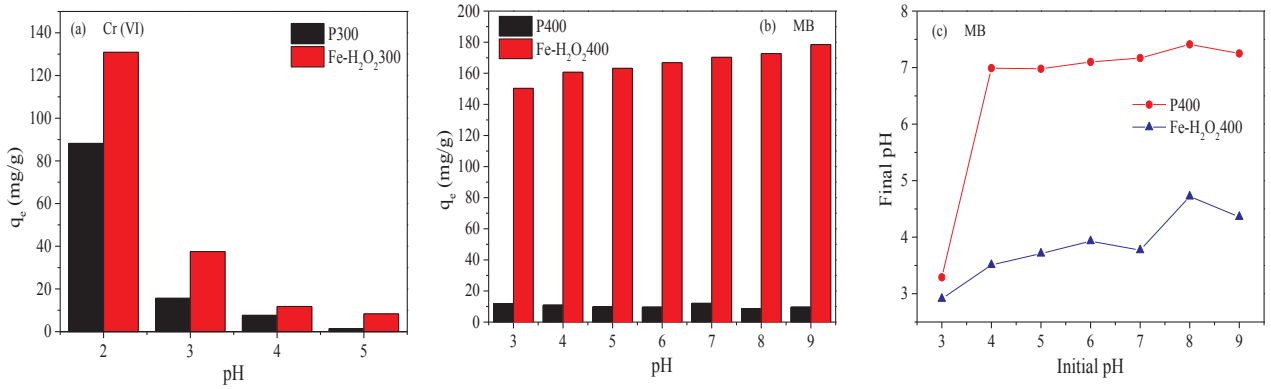


**Fig. 2.** Effect of initial pH on adsorption capabilities for Cr (VI) (200 mg/L, 1 g/L, 24 h, 25 ℃) and MB (100 mg/L, 0.5 g/L, 48 h; 25 ℃); and pH change of MB solution after adsorption (c).

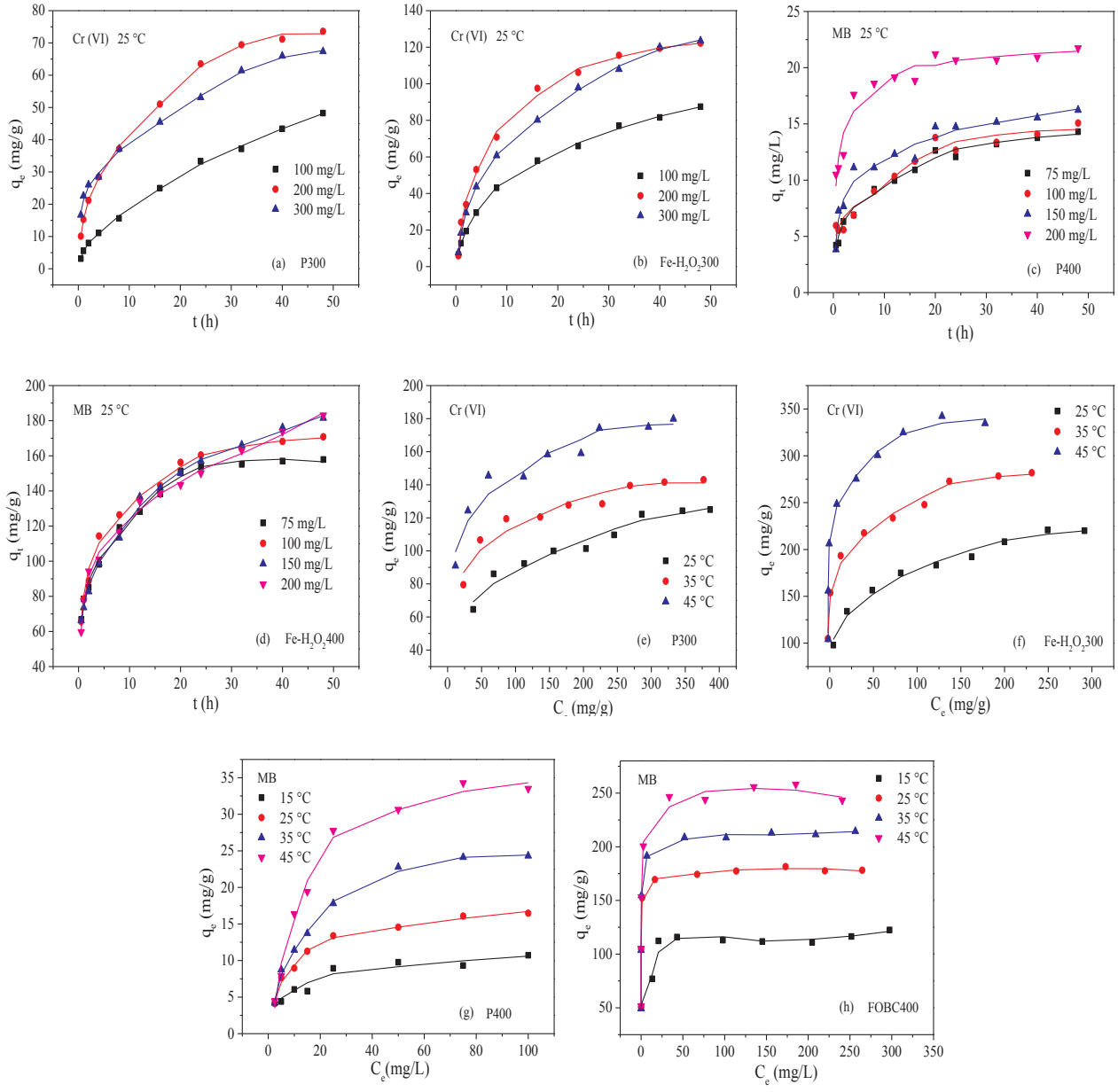


**Fig. 3.** Adsorption kinetics (a-d) and isotherms (e-h) of Cr (VI) (1 g/L, pH2) and MB (0.5 g/L, pH7).

FOBC300 completely disappeared probably ascribing to red shift and overlap by the peak at 1624 $cm^{-1}$ (Fig. 9d). As Cr (VI) and Cr (III) mainly existed in the forms of $HCrO_4^-$ and $Cr^{3+}$ at pH2, respectively (Zhou et al., 2016), the red shift should be resulted from hydrogen bonding of $HCrO_4^-$ and complexation of $Cr^{3+}$ with carboxyl. Thus, hydrogen bonding and complexation could be involved in the Cr (VI) and Cr (III) adsorptions, respectively. Moreover, $HCrO_4^-$ might be adsorbed above negatively charged surface at low pH and $Cr^{3+}$ could be exchanged with proton of acidic groups such as COOH and phenolic OH.

Similarly, the FTIR spectra of P400 and Fe-$H_2O_2$400 were measured after adsorption to elucidate the adsorption mechanism of MB. Little change was observed for P400 due to less adsorption of MB (E-supplementary data for this work can be found in e-version of this paper online). Instead, red shift was observed for COOH peak of Fe-$H_2O_2$400 (from 1707 to 1701 $cm^{-1}$) and two feature C-N peaks (Gong et al., 2015) of MB (from 1398 to 1387 $cm^{-1}$ and 1339 to 1329 $cm^{-1}$) (E-supplementary data for this work can be found in e-version of this paper online). Due to partial release of MB, the COOH peak slightly shifted from 1701 to 1705 $cm^{-1}$ after desorption. This demonstrated that hydrogen bonding was involved in the adsorption of Fe-$H_2O_2$400. pH obviously decreased after adsorption for Fe-$H_2O_2$400 as performing the adsorption at pH7 (Fig. 2c), indicating cation exchange between $H^+$ and MB cation occurred. Hence, carboxylic acids, which had strong cation exchange and hydrogen-bonding capabilities, should play an important role in the adsorption of MB. Additionally, cationic MB could also be adsorbed by electrostatic interaction of oxygen containing groups under natural conditions (Zhang et al., 2020). In brief, the generation of additional oxygen containing groups contributed to the increase of adsorption capability toward MB.

Iron oxides were less loaded on the surface of Fenton-modified biochars, contributed less to adsorption of Cr(VI) and MB. Therefore, the adsorption capabilities of Fenton-modified biochars were determined by biochar matrix. Considering only a small improvement in physical properties was obtained with Fenton modification (Table 1), the significant increase of adsorption capability toward Cr (VI) and MB

**Table 4**
The fitted parameters of adsorption kinetics and isotherms.

| Kinetics | | $C_o$ (mg/g) | $q_{e,exp}$ (mg/g) | PFOM : $\ln(q_e - q_t) = \ln q_e - k_1 t$ | | | PSOM: $\frac{t}{q_t} = \frac{1}{k_2 q_e^2} + \frac{1}{q_e} t$ | | |
|---|---|---|---|---|---|---|---|---|---|
| | | | | $q_{e,cal}$ | $k_1$ | $R^2$ | $q_{e,cal}$ | $k_2$ | $R^2$ |
| Cr (VI) | P300 | 100 | 48.25 | 47.29 | $5.11 \times 10^{-2}$ | 0.9718 | 57.97 | $1.16 \times 10^{-3}$ | 0.9212 |
| | | 200 | 73.59 | 66.67 | $8.22 \times 10^{-2}$ | 0.9907 | 81.97 | $1.88 \times 10^{-3}$ | 0.9852 |
| | | 300 | 67.35 | 56.48 | $7.80 \times 10^{-2}$ | 0.9205 | 71.23 | $2.87 \times 10^{-3}$ | 0.9749 |
| | Fe-$H_2O_2$300 | 100 | 87.48 | 79.20 | $6.27 \times 10^{-2}$ | 0.9896 | 99.30 | $1.12 \times 10^{-3}$ | 0.9863 |
| | | 200 | 122.20 | 108.71 | $8.87 \times 10^{-2}$ | 0.9926 | 141.44 | $9.48 \times 10^{-4}$ | 0.9896 |
| | | 300 | 123.59 | 120.90 | $7.59 \times 10^{-2}$ | 0.9404 | 143.27 | $7.51 \times 10^{-4}$ | 0.9870 |
| MB | P400 | 75 | 14.31 | 9.86 | $7.13 \times 10^{-2}$ | 0.9744 | 14.93 | $1.72 \times 10^{-2}$ | 0.9893 |
| | | 100 | 15.08 | 9.39 | $6.00 \times 10^{-2}$ | 0.8853 | 17.11 | $1.10 \times 10^{-2}$ | 0.9666 |
| | | 150 | 16.24 | 9.32 | $6.96 \times 10^{-2}$ | 0.9286 | 16.38 | $1.86 \times 10^{-2}$ | 0.9728 |
| | | 200 | 21.75 | 7.42 | $6.97 \times 10^{-2}$ | 0.7238 | 22.53 | $2.46 \times 10^{-2}$ | 0.9810 |
| | Fe-$H_2O_2$400 | 75 | 157.88 | 95.93 | $1.17 \times 10^{-1}$ | 0.9824 | 166.67 | $2.88 \times 10^{-3}$ | 0.9972 |
| | | 100 | 170.82 | 96.96 | $8.84 \times 10^{-2}$ | 0.9883 | 170.07 | $2.68 \times 10^{-3}$ | 0.9966 |
| | | 150 | 181.54 | 117.63 | $7.04 \times 10^{-2}$ | 0.9795 | 187.27 | $1.57 \times 10^{-3}$ | 0.9897 |
| | | 200 | 183.07 | 110.85 | $5.73 \times 10^{-2}$ | 0.9726 | 184.84 | $1.58 \times 10^{-3}$ | 0.9849 |

| Isotherms | | T (°C) | $q_{e,exp}$ (mg/g) | LM: $q_e = \frac{k_L q_{max} C_e}{1 + k_L C_e}$ | | | FM: $q_e = K_F C_e^{1/n}$ | | |
|---|---|---|---|---|---|---|---|---|---|
| | | | | $q_{max}$ | $K_L$ | $R^2$ | $K_F$ | 1/n | $R^2$ |
| Cr (VI) | P300 | 25 | 124.97 | 140.85 | 0.01802 | 0.9867 | 25.83 | 0.2672 | 0.9548 |
| | | 35 | 143.03 | 150.83 | 0.03870 | 0.9958 | 47.56 | 0.1901 | 0.9163 |
| | | 45 | 179.82 | 185.87 | 0.05036 | 0.9940 | 62.61 | 0.1843 | 0.9346 |
| | Fe-$H_2O_2$300 | 25 | 220.79 | 229.89 | 0.05158 | 0.9908 | 74.80 | 0.1911 | 0.9950 |
| | | 35 | 281.89 | 282.49 | 0.1676 | 0.9930 | 153.94 | 0.1065 | 0.9576 |
| | | 45 | 342.28 | 335.57 | 0.9313 | 0.9962 | 196.23 | 0.1084 | 0.9458 |
| MB | P400 | 15 | 10.72 | 10.62 | 0.2478 | 0.9876 | 4.86 | 0.1585 | 0.8332 |
| | | 25 | 16.47 | 16.65 | 0.3482 | 0.9958 | 7.37 | 0.1851 | 0.9815 |
| | | 35 | 24.32 | 25.01 | 0.3174 | 0.9946 | 10.22 | 0.1978 | 0.9688 |
| | | 45 | 34.28 | 34.00 | 0.7291 | 0.9972 | 17.43 | 0.1553 | 0.9876 |
| | Fe-$H_2O_2$400 | 15 | 122.56 | 119.47 | 0.2239 | 0.9959 | 72.96 | 0.0905 | 0.8648 |
| | | 25 | 178.18 | 178.90 | 2.5880 | 0.9998 | 114.98 | 0.0967 | 0.7708 |
| | | 35 | 214.48 | 213.68 | 1.4904 | 0.9999 | 126.37 | 0.1155 | 0.7991 |
| | | 45 | 258.14 | 249.38 | 10.0214 | 0.9985 | 142.88 | 0.1281 | 0.8676 |

should be primarily ascribed to introduction of new oxygen containing groups including –OH, C-O and –COOH.

### 3.2.6. Expansion of Fenton modification

When Fenton modification was applied to coconut shell biochar using 10 wt% $H_2O_2$, the adsorption capabilities of the biochars pyrolyzed at 300 and 400 °C were also greatly enhanced from 15.05 to 110.40 mg/g for Cr (VI) and from 6.81 to 205.05 mg/g for MB at 25 °C, respectively (Fig. 5a). The CFe-$H_2O_2$300 possessed inferior magnetic performance as the above Fe-$H_2O_2$300. Whereas, CFe-$H_2O_2$400 displayed 5.03 eum/g saturation magnetization, outperformed the corresponding Fe-modified biochar (CFe400: 3.77 eum/g) (Fig. 5b). This further proved that Fenton modification was subjected to pyrolysis temperature for enhancing saturation magnetization of biochar. Importantly, a good saturation magnetization could be obtained with Fenton-modification, guaranteeing magnetic separation of biochar after adsorption.

## 4. Conclusion

A highly efficient strategy was established for improving the adsorptive and magnetic capabilities of biochar by combining $FeCl_3$-promoted pyrolysis and $H_2O_2$ oxidation (Fenton modification). The adsorption capabilities of rubber tree bark biochars toward Cr (VI) and

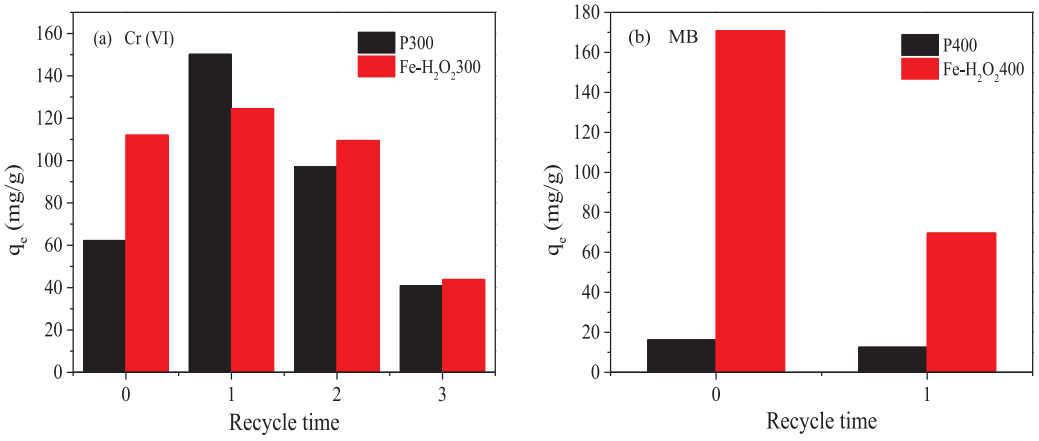


**Fig. 4.** The adsorption capability of regenerated biochar for Cr (VI) (200 mg/L, 1.0 g/L, pH2, 48 h, 25 °C) and MB (100 mg/L, 0.5 g/L, pH7, 24 h, 25 °C).

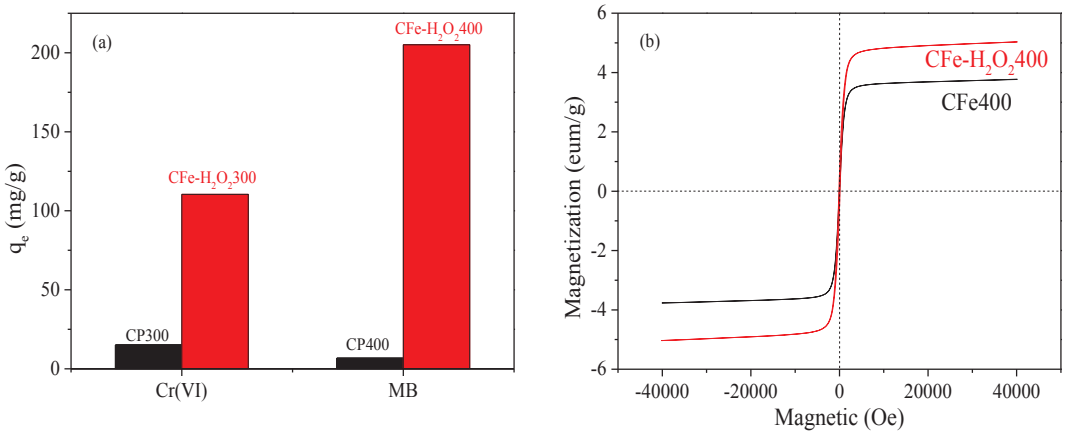


**Fig. 5.** The adsorption capabilities (a) (Cr (VI): 200 mg/L, 1 g/L, pH2, 48 h; MB: 200 mg/L, 0.5 g/L, pH7, 48 h) and magnetic hysteresis loops (b) of coconut shell biochar.

MB were enormously upgraded due to introduction of oxygen-containing groups. The saturation magnetization of magnetic biochar could also be enhanced by transforming nonmagnetic iron species into ϒ-$Fe_2O_3$. Moreover, this modification brought great enhancement in the adsorptive and magnetic capabilities of coconut shell biochar. This demonstrated that Fenton modification should be a general and efficient technology for improving the adsorptive and magnetic capabilities of biochar.

## CRediT authorship contribution statement

**Shuang Xu:** Investigation, Data curation, Writing - original draft. **Jihui Li:** Conceptualization, Methodology, Writing - review & editing, Project administration. **Zhibing Yin:** Investigation, Visualization. **Sen Liu:** Investigation. **Siyao Bian:** Data curation. **Yucang Zhang:** Resources, Supervision.

## Declaration of Competing Interest

The authors declare that they have no known competing financial interests or personal relationships that could have appeared to influence the work reported in this paper.

## Acknowledgements

The Hainan Provincial Natural Science Foundation of China (519QN175), National Natural Science Foundation of China (21801053) and National Medium- and Long-term Science and Technology Development Program of China (ZY2018HN09-4) were acknowledged.

## Appendix A. Supplementary data

Supplementary data to this article can be found online at https://doi.org/10.1016/j.biortech.2020.123797.

## References

Chen, T., Zhou, Z., Xu, S., Wang, H., Lu, W., 2015. Adsorption behavior comparison of trivalent and hexavalent chromium on biochar derived from municipal sludge. Bioresour. Technol. 190, 388–394.
Daneshvar, E., Vazirzadeh, A., Niazi, A., Sillanpää, M., Bhatnagar, A., 2017. A comparative study of methylene blue biosorption using different modified brown, red and green macroalgae – Effect of pretreatment. Chem. Eng. J. 307, 435–446.
Devi, P., Saroha, A.K., 2014. Synthesis of the magnetic biochar composites for use as an adsorbent for the removal of pentachlorophenol from the effluent. Bioresour. Technol. 169, 525–531.
Ding, Z., Hu, X., Wan, Y., Wang, S., Gao, B., 2016. Removal of lead, copper, cadmium, zinc, and nickel from aqueous solutions by alkali-modified biochar: Batch and column tests. J. Ind. Eng. Chem. 33, 239–245.
Duan, S., Ma, W., Pan, Y., Meng, F., Yu, S., Wu, L., 2017. Synthesis of magnetic biochar from iron sludge for the enhancement of Cr (VI) removal from solution. J. Taiwan Inst. Chem. Eng. 80, 835–841.
Gong, J., Liu, J., Jiang, Z., Wen, X., Mijowska, E., Tang, T., Chen, X., 2015. A facile approach to prepare porous cup-stacked carbon nanotube with high performance in adsorption of methylene blue. J. Colloid. Interf. Sci. 445, 195–204.
Han, Y., Cao, X., Ouyang, X., Sohi, S.P., Chen, J., 2016. Adsorption kinetics of magnetic biochar derived from peanut hull on removal of Cr (VI) from aqueous solution: Effects of production conditions and particle size. Chemosphere 145, 336–341.
Huff, M.D., Lee, J.W., 2016. Biochar-surface oxygenation with hydrogen peroxide. J. Environ. Manage. 165, 17–21.
Karunanayake, A.G., Todd, O.A., Crowley, M., Ricchetti, L., Pittman, C.U., Anderson, R., Mohan, D., Mlsna, T., 2018. Lead and cadmium remediation using magnetized and nonmagnetized biochar from Douglas fir. Chem. Eng. J. 331, 480–491.
Kırboğa, S., Öner, M., 2009. Inhibition of calcium oxalate crystallization by graft copolymers. Cryst. Growth Des. 9, 2159–2167.
Lai, Y., Jiao, Y., Song, J., Zhang, K., Li, J., Zhang, Z., 2018. Fe/$Fe_3C$@graphitic carbon shell embedded in carbon nanotubes derived from Prussian blue as cathodes for Li-$O_2$ batteries. Mater. Chem. Front. 2, 376–384.
Liu, W., Ni, J., Yin, X., 2014. Synergy of photocatalysis and adsorption for simultaneous removal of Cr (VI) and Cr (III) with $TiO_2$ and titanate nanotubes. Water Res. 53, 12–25.
Lyu, H., Xia, S., Tang, J., Zhang, Y., Gao, B., Shen, B., 2020. Thiol-modified biochar synthesized by a facile ball-milling method for enhanced sorption of inorganic $Hg^{2+}$ and organic $CH_3Hg^+$. J. Hazard. Mater. 384, 121357.
Ma, Y., Liu, W.J., Zhang, N., Li, Y.S., Jiang, H., Sheng, G.P., 2014. Polyethylenimine modified biochar adsorbent for hexavalent chromium removal from the aqueous solution. Bioresour. Technol. 169, 403–408.
Mandal, S., Sarkar, B., Bolan, N., Ok, Y.S., Naidu, R., 2017. Enhancement of chromate reduction in soils by surface modified biochar. J. Environ. Manage. 186, 277–284.
Manning, B.A., Kiser, J.R., Kwon, H., Kanel, S.R., 2007. Spectroscopic investigation of Cr (III)- and Cr (VI)-treated nanoscale zerovalent iron. Environ. Sci. Technol. 41, 586–592.
Mian, M.M., Liu, G., Yousaf, B., Fu, B., Ullah, H., Ali, M.U., Abbas, Q., Mujtaba Munir, M.A., Ruijia, L., 2018. Simultaneous functionalization and magnetization of biochar via $NH_3$ ambiance pyrolysis for efficient removal of Cr (VI). Chemosphere 208, 712–721.
Mohan, D., Kumar, H., Sarswat, A., Alexandre-Franco, M., Pittman, C.U., 2014a. Cadmium and lead remediation using magnetic oak wood and oak bark fast pyrolysis bio-chars. Chem. Eng. J. 236, 513–528.
Mohan, D., Kumar, S., Srivastava, A., 2014b. Fluoride removal from ground water using magnetic and nonmagnetic corn stover biochars. Ecol. Eng. 73, 798–808.
Mubarak, N.M., Fo, Y.T., Al-Salim, H.S., Sahu, J.N., Abdullah, E.C., Nizamuddin, S., Jayakumar, N.S., Ganesan, P., 2015. Removal of methylene blue and orange-G from waste water using magnetic biochar. Int. J. Nanosci. 14, 1550009.
Nair, V., Vinu, R., 2016. Peroxide-assisted microwave activation of pyrolysis char for adsorption of dyes from wastewater. Bioresour. Technol. 216, 511–519.
Nasuha, N., Hameed, B.H., 2011. Adsorption of methylene blue from aqueous solution onto NaOH-modified rejected tea. Chem. Eng. J. 166, 783–786.
Ouyang, J.-M., Deng, S.-P., Zhong, J.-P., Tieke, B., Yu, S.-H., 2004. Crystallization of calcium oxalate monohydrate at dipalmitoylphosphatidylcholine monolayers in the presence of chondroitin sulfate A. J. Cryst. Growth 270, 646–654.
Özçimen, D., Ersoy-Meriçboyu, A., 2010. Characterization of biochar and bio-oil samples obtained from carbonization of various biomass materials. Renew. Energ. 35, 1319–1324.
Pradhan, D., Sukla, L.B., Sawyer, M., Rahman, P.K.S.M., 2017. Recent bioreduction of hexavalent chromium in wastewater treatment: A review. J. Ind. Eng. Chem. 55, 1–20.
Qada, E.E.N., Allen, S.J., Walker, G.M., 2006. Adsorption of methylene blue onto activated carbon produced from steam activated bituminous coal: A study of equilibrium

adsorption isotherm. Chem. Eng. J. 124, 103–110.
Reguyal, F., Sarmah, A.K., Gao, W., 2017. Synthesis of magnetic biochar from pine sawdust via oxidative hydrolysis of $FeCl_2$ for the removal sulfamethoxazole from aqueous solution. J. Hazard. Mater. 321, 868–878.
Shi, S., Yang, J., Liang, S., Li, M., Gan, Q., Xiao, K., Hu, J., 2018. Enhanced Cr(VI) removal from acidic solutions using biochar modified by $Fe_3O_4$@$SiO_2$-$NH_2$ particles. Sci. Total Environ. 628–629, 499–508.
Song, Z., Lian, F., Yu, Z., Zhu, L., Xing, B., Qiu, W., 2014. Synthesis and characterization of a novel MnOx-loaded biochar and its adsorption properties for $Cu^{2+}$ in aqueous solution. Chem. Eng. J. 242, 36–42.
Tan, Y.-H., Ouyang, J.-M., Ma, J., Feng, H.-H., Feng, H., 2003. The application of infrared spectrophotometry on the study of calcium oxalate calculi. Spectrosc. Spect. Anal. 23, 700–704.
Tan, Z., Qiu, J., Zeng, H., Liu, H., Xiang, J., 2011. Removal of elemental mercury by bamboo charcoal impregnated with $H_2O_2$. Fuel 90, 1471–1475.
Trakal, L., Veselska, V., Safarik, I., Vitkova, M., Cihalova, S., Komarek, M., 2016. Lead and cadmium sorption mechanisms on magnetically modified biochars. Bioresour. Technol. 203, 318–324.
Wang, Q., Wang, B., Lee, X., Lehmann, J., Gao, B., 2018. Sorption and desorption of Pb(II) to biochar as affected by oxidation and pH. Sci. Total Environ. 634, 188–194.
Wang, S., Gao, B., Li, Y., Creamer, A.E., He, F., 2017. Adsorptive removal of arsenate from aqueous solutions by biochar supported zero-valent iron nanocomposite: Batch and continuous flow tests. J. Hazard. Mater. 322, 172–181.
Wang, S., Zhao, M., Zhou, M., Li, Y.C., Wang, J., Gao, B., Sato, S., Feng, K., Yin, W., Igalavithana, A.D., Oleszczuk, P., Wang, X., Ok, Y.S., 2019. Biochar-supported nZVI (nZVI/BC) for contaminant removal from soil and water: A critical review. J. Hazard. Mater. 373, 820–834.
Xiong, T., Yuan, X., Chen, X., Wu, Z., Wang, H., Leng, L., Wang, H., Jiang, L., Zeng, G., 2018. Insight into highly efficient removal of cadmium and methylene blue by eco-friendly magnesium silicate-hydrothermal carbon composite. Appl. Surf. Sci. 427, 1107–1117.
Xue, Y., Gao, B., Yao, Y., Inyang, M., Zhang, M., Zimmerman, A.R., Ro, K.S., 2012. Hydrogen peroxide modification enhances the ability of biochar (hydrochar) produced from hydrothermal carbonization of peanut hull to remove aqueous heavy metals: Batch and column tests. Chem. Eng. J. 200–202, 673–680.
Yang, F., Zhang, S., Sun, Y., Cheng, K., Li, J., Tsang, D.C.W., 2018. Fabrication and characterization of hydrophilic corn stalk biochar-supported nanoscale zero-valent iron composites for efficient metal removal. Bioresour. Technol. 265, 490–497.
Yao, F.X., Arbestain, M.C., Virgel, S., Blanco, F., Arostegui, J., Macia-Agullo, J.A., Macias, F., 2010. Simulated geochemical weathering of a mineral ash-rich biochar in a modified Soxhlet reactor. Chemosphere 80, 724–732.
Yi, Y., Huang, Z., Lu, B., Xian, J., Tsang, E.P., Cheng, W., Fang, J., Fang, Z., 2020. Magnetic biochar for environmental remediation: A review. Bioresour. Technol. 298, 122468.
Yin, Z., Xu, S., Liu, S., Xu, S., Li, J., Zhang, Y., 2020. A novel magnetic biochar prepared by $K_2FeO_4$-promoted oxidative pyrolysis of pomelo peel for adsorption of hexavalent chromium. Bioresour. Technol. 300, 122680.
Zhang, M., Gao, B., 2013. Removal of arsenic, methylene blue, and phosphate by biochar/AlOOH nanocomposite. Chem. Eng. J. 226, 286–292.
Zhang, M., Gao, B., Varnoosfaderani, S., Hebard, A., Yao, Y., Inyang, M., 2013. Preparation and characterization of a novel magnetic biochar for arsenic removal. Bioresour. Technol. 130, 457–462.
Zhang, P., O'Connor, D., Wang, Y., Jiang, L., Xia, T., Wang, L., Tsang, D.C.W., Ok, Y.S., Hou, D., 2020. A green biochar/iron oxide composite for methylene blue removal. J. Hazard. Mater. 384, 121286.
Zhao, N., Yin, Z., Liu, F., Zhang, M., Lv, Y., Hao, Z., Pan, G., Zhang, J., 2018. Environmentally persistent free radicals mediated removal of Cr(VI) from highly saline water by corn straw biochars. Bioresour. Technol. 260, 294–301.
Zhi, J., Zhao, W., Liu, X., Chen, A., Liu, Z., Huang, F., 2014. Highly conductive ordered mesoporous carbon based electrodes decorated by 3D graphene and 1D silver nanowire for flexible supercapacitor. Adv. Funct. Mater. 24, 2013–2019.
Zhou, L., Liu, Y., Liu, S., Yin, Y., Zeng, G., Tan, X., Hu, X., Hu, X., Jiang, L., Ding, Y., Liu, S., Huang, X., 2016. Investigation of the adsorption-reduction mechanisms of hexavalent chromium by ramie biochars of different pyrolytic temperatures. Bioresour. Technol. 218, 351–359.
Zhou, Y., Gao, B., Zimmerman, A.R., Chen, H., Zhang, M., Cao, X., 2014. Biochar-supported zerovalent iron for removal of various contaminants from aqueous solutions. Bioresour. Technol. 152, 538–542.
Zhu, Y., Zhu, R., Xi, Y., Zhu, J., Zhu, G., He, H., 2019. Strategies for enhancing the heterogeneous Fenton catalytic reactivity: A review. Appl. Catal. B: Environ. 255, 117739.
Zuo, X., Liu, Z., Chen, M., 2016. Effect of $H_2O_2$ concentrations on copper removal using the modified hydrothermal biochar. Bioresour. Technol. 207, 262–267.